Porous Self-Assembled Molecular Networks as Templates for Chiral Position-Controlled Chemical Functionalization of Graphitic Surfaces

Kazukuni Tahara,*[,1,2,4] Yuki Kubo,[1] Shingo Hashimoto,[2] Toru Ishikawa,[1] Hiromasa Kaneko,[2] Anton Brown,[3] Brandon E. Hirsch,[3] Steven De Feyter,*[,3] Yoshito Tobe,*[,1,5,6]

[1] Division of Frontier Materials Science, Graduate School of Engineering Science, Osaka University, Toyonaka, Osaka 560-8531, Japan.

[2] Department of Applied Chemistry, School of Science and Technology, Meiji University, 1-1-1 Higashimita, Tama-ku, Kawasaki, Kanagawa, 214-8571, Japan.

[3] Division of Molecular Imaging and Photonics, Department of Chemistry, KU Leuven, Celestijnenlaan 200F, 3001 Leuven, Belgium.

[4] PRESTO, Japan Science and Technology Agency, 4-1-8, Honcho, Kawaguchi, Saitama 332-0012, Japan.

[5] The Institute of Scientific and Industrial Research, Osaka University, Ibaraki, Osaka 567-0047, Japan.

[6] Department of Applied Chemistry, National Chiao Tung University, 1001 Ta Hsueh Road, Hsinchu 30010, Taiwan.

ABSTRACT:

Controlled covalent functionalization of graphitic surfaces with molecular scale precision is crucial for tailored modulation of the chemical and physical properties of carbon materials. We herein present that porous self-assembled molecular networks (SAMNs) act as nanometer scale template for the covalent electrochemical functionalization of graphite using an aryldiazonium salt. Hexagonally aligned achiral grafted species with lateral periodicity of 2.3, 2.7, and 3.0 nm were achieved utilizing SAMNs having different pore-to-pore distances. The unit cell vectors of the grafted pattern match those of the SAMN. After the covalent grafting, the template SAMNs can be removed by simple washing with a common organic solvent. We briefly discuss the mechanism of the observed pattern transfer. The unit cell vectors of the grafted pattern align along non-symmetry axes of graphite, leading to mirror-image grafted domains, in accordance with the domain-specific chirality of the template. In case a homochiral building block is used for SAMN formation, one of the 2D mirror image grafted patterns is cancelled. This is the first example of a nearly crystalline one-sided or supratopic covalent chemical functionalization. In addition, the positional control imposed by the SAMN renders the functionalized surface (homo)chiral reaching a novel level of control for the functionalization of carbon surfaces, including surface-supported graphene.

INTRODUCTION

Controlling surfaces' chemical and physical properties by covalent modification has attracted intense interest in view of applications in molecular electronics,[1–3] supercapacitors and batteries,[4,5] sensors,[6] surface patterning[7] and inks.[8] While most covalent surface modification strategies do not render spatial control on the nanoscale, the development of surface functionalization methods to nanopattern with molecular level precision is highly desirable.[9–11] Such is very challenging as covalent surface functionalization often relies on high energy reagents or harsh reaction conditions that produce rather ill-defined nanoscale surface structures,[12–16] though for some selected systems atomic precision was achieved.[17,18] Aryldiazonium chemistry is amongst the most popular ones to covalently functionalize a variety of surfaces,[19,20] particularly carbon surfaces.[21] Homolytic dediazotization via (electro)chemical reduction of the aryldiazonium ions generates aryl radicals that attack nearby to form covalent bonds with the surface (Figure 1a).[22] This approach has been employed to introduce various chemical functionalities on surfaces, while the functional groups of aryl diazonium salts affect the grafting density as well as thickness of the resulting film.[23–26] Organizational control, yet at the (sub)micrometer scale, of this aryldiazonium covalent chemistry on carbon surfaces is known using polystyrene bead templates,[27,28] microfluidic flow systems,[29] and lithographic stamps.[30,31] Recently, an approach based on the formation of nanobubbles that act as masks was reported.[32] Toward spatial control at the molecular scale, an interesting approach involving the preassembly of reactive aryldiazonium precursors is reported.[33]

We recently introduced a unique approach for the template-guided one-dimensional (1D) covalent functionalization of graphite or graphene using aryldiazonium chemistry.[34] High-density self-assembled molecular networks (SAMNs) of long alkanes, *e.g.* triacontane, tetracontane, and pentacontane, effectively acted as removable templates to produce surfaces with parallel rows of grafted molecules, only few nanometers wide. The average distance between parallel grafted rows is dictated by the length of the alkane molecules. Such linearized grafting using high-density SAMN templates might actually be a rather special case of the scope that SAMN templates offer to guide

covalent grafting. Selection of relevant SAMN templates is made possible thanks to the accumulated knowledge of two-dimensional (2D) molecular self-assembly at liquid/solid interfaces.[35,36] In this respect, the development of other covalent pattern symmetries is definitely a relevant research goal. In particular, porous molecular networks are of special interest for two reasons.[37–39] The first reason is a conceptual one. In contrast to the high-density alkane SAMNs, their intrinsic porosity should facilitate the templated grafting, namely in the supramolecular pores. In this respect, the seminal work of Buck and co-workers using porous self-assembled molecular networks on gold, though as template for the area-selective surface modification by self-assembling thiolates, supports the concept.[40] It should be noted though that in this case no covalent grafting was involved. The second reason is that it is known that several of these porous self-assembled networks form lattices with a distinct handedness on graphite and graphene.[41,42] The use of such template monolayer for covalent grafting may lead to (homo)chiral surfaces, with potential for optical, electronical, sensing, and catalytic applications.[43,44]

Herein we present the formation of covalently functionalized graphite surfaces of hexagonal symmetry with grafted molecules in different periodicities using self-assembled porous networks as the templating masks (Figure 1b). As templates, we chose porous molecular networks formed by alkoxy-substituted dehydrobenzo[12]annulene (DBA) derivatives (**DBA-OCn**s) at the liquid/graphite interface (Figure 1c).[45–47] These molecules produce honeycomb type porous structures through van der Waals interactions of the interdigitated alkyl chains (Figures 1c). The pore diameter, and also pore-to-pore distance can be tuned just by changing the alkyl chain length.[45,46] Moreover, the DBA honeycomb networks show a clear handedness by virtue of combination of specific (point group) molecular chirality and the arrangement of their interdigitated alkyl chains (*i.e.* organizational or supramolecular chirality, Figure 2).[41] Furthermore, and also of more relevance for this study, is the handedness in the lateral orientation of the DBA SAMNs with respect to the graphite lattice, as expressed by the orientation of their unit cells vectors with respect to the unit cell vectors or symmetry axes of the graphite lattice.[48]

As an aryl radical source, 3,4,5-trimethoxybenzenediazonium (TMeOD) chloride was chosen because the corresponding aryl radical attacks the graphite surface with a very high grafting density (Figure 1a).[21,26] During electrochemical (EC) treatment, a phase separated solution double layer was employed to ensure formation of extended domains of the DBA networks.[34] Patterning periodicities of the covalently bound molecular units could be controlled to 2.3, 2.7, and 3.0 nm using SAMNs with different pore-to-pore distances formed by **DBA-OCn**s (*i.e.* **DBA-OC4**, **DBAO-C6**, and **DBA-OC8**). Pattern transfer fidelity and plausible mechanism are also discussed. Moreover, the unit cell vectors of the pattern formed by the pore centers of the template layer, and therefore also of the grafted molecules lie along non-symmetry axes of the substrate underneath. Using a chiral DBA derivative (**cDBA-OC6-OC6(*S*)**), which in contrast to the achiral **DBA-OCn**s forms a template layer of single handedness (Figure 1d), renders the one-sided or supratopic *functionalized* carbon surface homochiral (*vide infra*).[49]

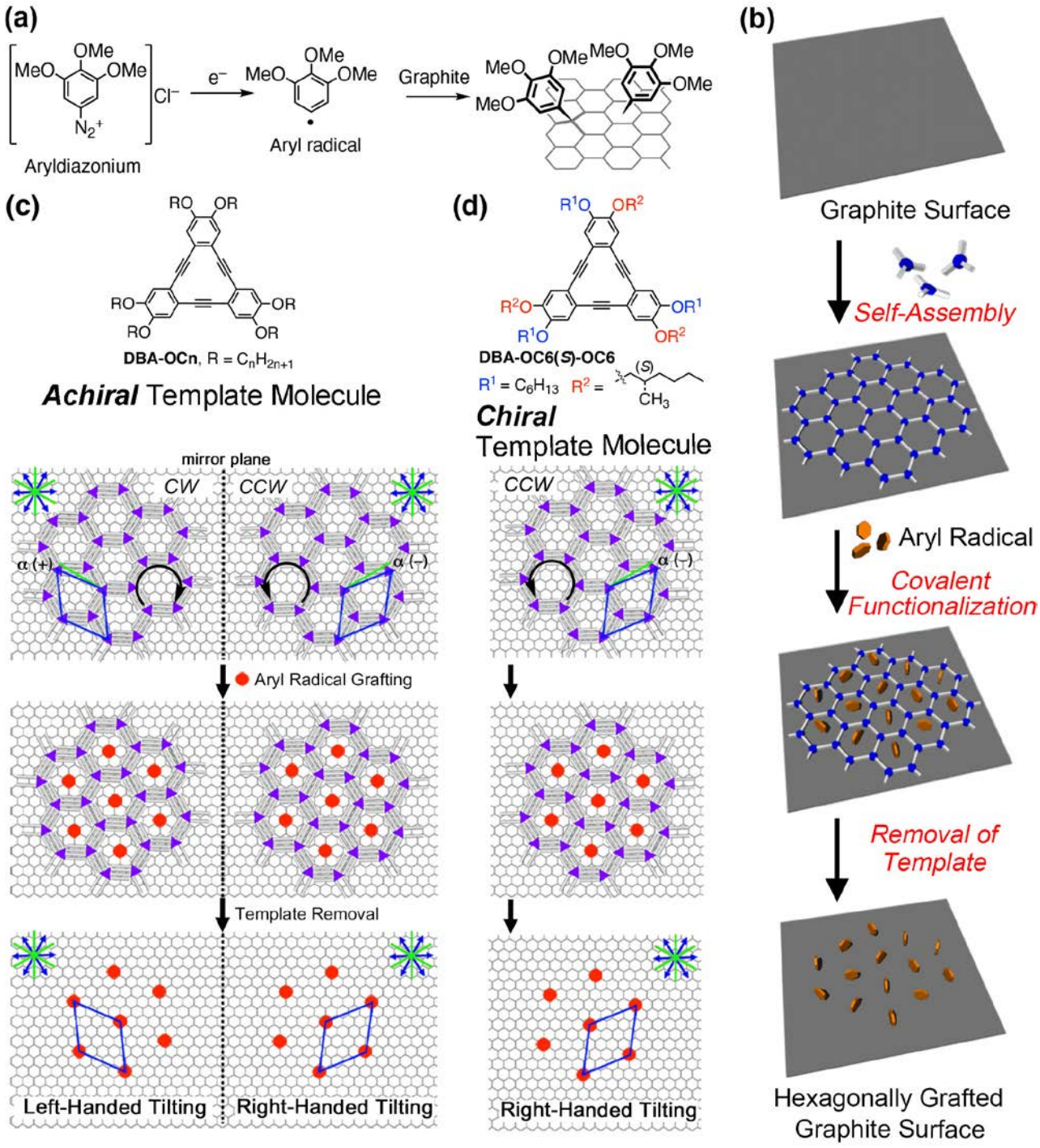

Figure 1. (a) Covalent surface functionalization of a graphite surface using an aryldiazonium TMeOD ion having three methoxy groups at 3,4,5-positions. (b) Schematic drawing of the porous template-guided hexagonal grafting. (c) Chemical structure of achiral **DBA-OCn** and schematic drawing of the porous template-guided hexagonal grafting on top of a honeycomb graphene/graphite lattice. Blue arrows are the main symmetry axes of graphene/graphite, while the light green ones represent their normals. The purple triangles represent the DBA cores, while the faint lines connected to them are the alkyl chains. The alkyl chains of adjacent DBA molecules are interdigitated. Blue rhombi are

the unit cells of the supramolecular template networks and those for the grafted species (assuming grafting in the center of the pores). The supramolecular template network belongs to plane group *p*6 and is therefore chiral, giving rise to mirror-image counter-clockwise (*CCW*, left) and clockwise (*CW*, right) patterns.[50] The resulting pattern of the grafted molecules (red dots) is achiral (plane group *p*6m). Nevertheless, the angle between the SAMN unit cell vectors (blue rhombi) and the directions normal to the main symmetry axes of graphite (indicated in light green) is non-zero. This off-set renders the one-sided or supratopic functionalized surface locally chiral. (d) Chemical structure of **cDBA-OC6(*S*)-OC6** and schematic drawing of the porous template-guided hexagonal grafting using **cDBA-OC6(*S*)-OC6** which forms supramolecular template layers of unique handedness, rendering the supratopic functionalized surface globally chiral. For clarity, in (c) and (d), the unit cell vectors of the SAMN and grafted pattern, and the graphite lattice are not to scale.

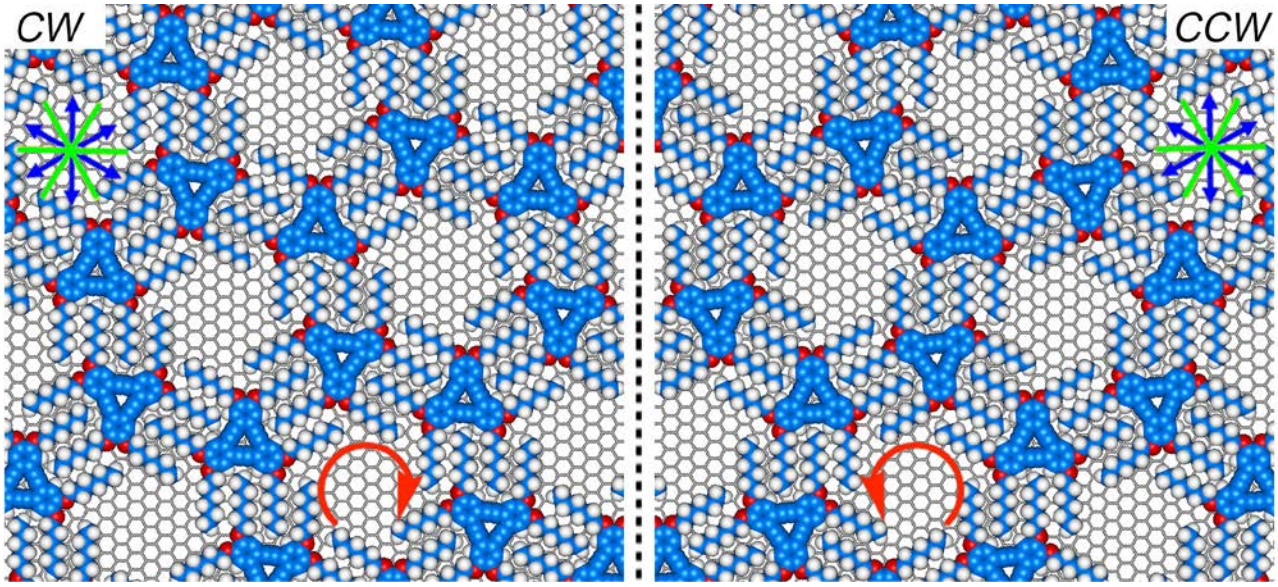

Figure 2. Models of self-assembled molecular networks of different handedness (plane group *p*6),[50] called counter-clockwise (*CCW*, left) and clockwise (*CW*, right) as defined by the orientation of the inner alkoxy chains in the pore, formed by **DBAOC6** on the topmost graphene layer of a graphite substrate. The blue arrows and light green lines represent the main symmetry axes of graphite, and the directions normal to those.

RESULTS AND DISCUSSION

Porous Self-Assembled Monolayers Formed by DBA-OCns (n = 4, 6, and 8)

To investigate the optimal conditions for the porous template network formation, self-assembling behavior of **DBA-OCn**s (n = 4, 6, and 8) at the 1-phenyloctane/graphite interface was observed by means of scanning tunneling microscopy (STM). Molecular modeling shows that the pore sizes of the DBA honeycomb structures are slightly too small for **DBA-OC4**, optimal for **DBA-OC6**, and slightly too large for **DBA-OC8**, to accommodate one trimethoxyphenyl group (Figure S1). 1-Phenyloctane was chosen as the solvent because it is suitable as an interfacial masking layer thanks to its non-polar, non-volatile properties alongside its inert chemical behavior under the experimental conditions. The concentration of the DBA solutions is kept low (5.0×10^{-5} M for **DBA-OC4**, 2.0×10^{-5} M for **DBA-OC6**, and 6.0×10^{-6} M for **DBA-OC8**) to ensure the formation of the low-density porous honeycomb structure.[46,47] After adding the relevant solution (30 μL) to a liquid cell placed on the basal plane of a 1 cm × 1 cm piece of highly oriented pyrolytic graphite, the sample was annealed at 80 °C for 1 h in a sealed oven to enlarge the size of the **DBA-OCn** 2D monolayer crystals. All STM images were recorded at the 1-phenyloctane/graphite interface at room temperature.

Figure 3 display STM images of SAMNs formed by **DBA-OC6**. In the STM images, bright features correspond to the triangular π-conjugated cores of the DBAs, darker parts connecting the DBA cores are composed of the four interdigitated alkyl chains,[51] revealing the formation of honeycomb structures. The alkyl chains of the DBAs lie parallel to the main symmetry axes of the underlying graphite surface. The typical domain sizes are over 200 nm × 200 nm. Unit cell parameters are a = b = 3.2 ± 0.1 nm and γ = 60 ± 1° for **DBA-OC6** (Table S1). The shortest pore-to-pore distance (diagonal lines of the unit cell) is 2.8 ± 0.1 nm. For these achiral DBAs, both mirror-image *CW* and *CCW* honeycomb domains appear with equal probability (Figures 3b and c). Angles α between the unit cell vector and the normals of graphite are 6.3 ± 0.7° and –6.3 ± 0.7° for the *CW* and *CCW* structures, respectively.[48,52] Similarly, the other DBAs also form extended domains of chiral honeycomb structures at the 1-phenyloctane/graphite interface (Figures S2 and S3). Unit cell

parameters are a = b = 2.8 ± 0.1 nm and γ = 60 ± 1° and a = b = 3.6 ± 0.1 nm and γ = 60 ± 1°, and the shortest pore-to-pore distances are 2.4 ± 0.1 nm and 3.2 ± 0.1 nm, for **DBAOC4** and **DBAOC8**, respectively. The angles α are ±8.8 ± 0.7° for the structures of **DBA-OC4** and ±5.9 ± 0.7° for the structures of **DBA-OC8**, respectively.

To model the network structures, molecular mechanics (MM) simulations of the DBA networks with COMPASS force field are performed, by employing unit cell parameters as periodic boundary conditions, on a two-layer sheet of graphene (interlayer distance is 0.335 nm) which represents graphite. Optimized network models are displayed in Figure S4. From these model structures, we estimated the pore sizes based on the averaged interatomic distances between the carbon atoms at the end of the alkoxy chains located at the rim of the hexagonal pores. Following this procedure, the pore diameter is 1.2 nm for **DBA-OC4**, 1.6 nm for **DBA-OC6**, and 2.0 nm for **DBA-OC8**, respectively (Table S1).

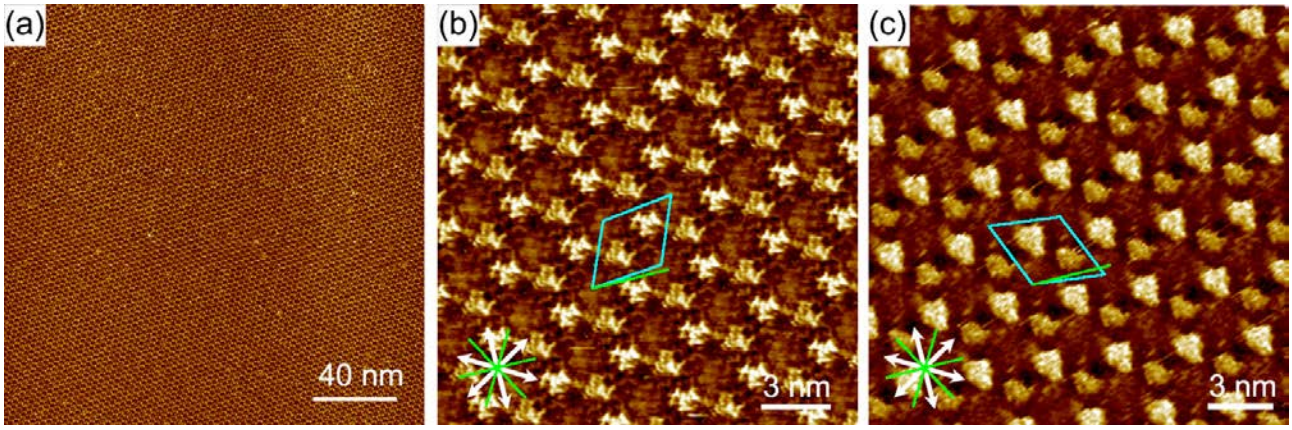

Figure 3. STM images of SAMNs of **DBA-OC6** at the 1-phenyloctane/graphite interface (V_{bias} = −0.55 V, I_{set} = 30 pA). (a) Large area image showing an extended domain covering the whole image. (b) Small area image of the *CW* structure (V_{bias} = −0.60 V, I_{set} = 100 pA). (c) Small area image of the *CCW* structure (V_{bias} = −0.33 V, I_{set} = 50 pA). White arrows and light green lines are main symmetry axes of the graphite substrate underneath, and the in-plane directions normal to those, respectively. Turquoise rhombi in the images (b) and (c) are unit cells. Angles α are between one of the unit cell

vectors and the closest normal. Clockwise or counter-clockwise rotation of the unit cell vectors to the normal are expressed by + or – signs of the angle α, respectively.

Templated Grafting at Double Layer Conditions

First, chemical functionalization of the graphite surface through EC reduction of TMeOD in phase separated solution double layer conditions, *i.e.*, in the presence of a thin organic solvent layer between the graphite working electrode and the aqueous electrolyte, was checked without the templating mask. As an interfacial layer, 1-phenyloctane (30 μL) was used. After the addition of an aqueous TMeOD solution onto the 1-phenyloctane layer, EC reduction was carried out in a cyclic voltammogram (CV) mode (a single cycle from +0.20 to –0.25 V, vs. Ag/AgCl, 0.1 V/s). A large irreversible reduction peak appeared at –0.15 V (Figure 4a), which agrees with the reduction potential of the TMeOD ion without the interfacial layer.[26] After the EC functionalization, the graphite surface was subjected to spectroscopic characterization using Raman spectroscopy with excitation laser wavelength of 532 nm (Figure 4b). The appearance of the graphite defect band (D-peak) at 1350 cm^{-1} confirms surface covalent bond formation.[53] A ratiometric intensity comparison of the D-peak to the G-peak appearing at 1580 cm^{-1} yields an I_D/I_G value that is representative of the degree of the covalent grafting. The I_D/I_G value of this sample is 0.074 ± 0.001. Local structural analysis of the functionalized graphite surface by means of STM at the 1-phenyloctane/graphite interface revealed that there are numerous bright features that are assigned to individual trimethoxyphenyl molecular units (Figure 4c).[25,26] A two-dimensional Fast Fourier Transform (2D-FFT) image (Figure 4c: inset) only shows a large dim bright round feature, confirming positionally non-controlled grafting. Electrochemistry, Raman spectroscopy and STM observation support that covalent grafting of TMeOD takes places through the interfacial 1-phenyloctane layer.

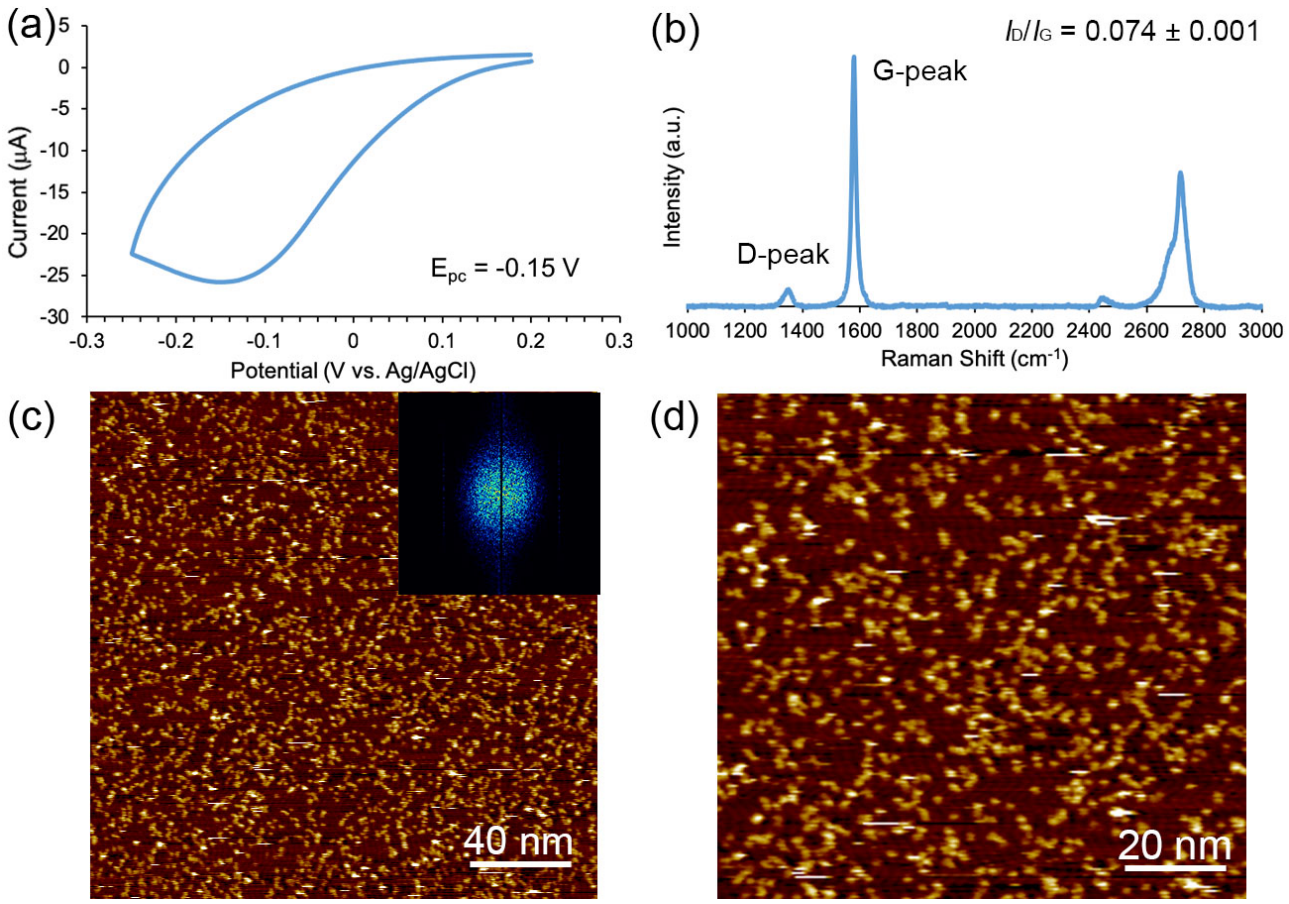

Figure 4. (a) Cyclic voltammogram during EC grafting of graphite using TMeOD under solution double layer conditions (a single cycle from +0.20 to –0.25 V, vs. Ag/AgCl, 0.1 V/sec). 1-Phenyloctane was used as the organic solvent layer. (b) Raman spectrum after drying the surface. Excitation laser wavelength is 532 nm. Mean I_D/I_G is 0.074 ± 0.001. (c) STM image of the functionalized graphite surface recorded at the 1-phenyloctane/graphite interface (V_{bias} = −0.80 V, I_{set} = 30 pA). The inset is the corresponding 2D-FFT image, showing no periodicity of the bright features. (d) Digital zoom of the image (c).

Table 1. Summary of the Reduction Potentials of TMeOD Ion in the Cyclic Voltammograms (CV), Mean I_D/I_G Calculated by Raman Spectra of the Functionalized Surface, and the Pore-to-Pore Distances Determined from Two-Dimensional Fast Fourier Transform (2D-FFT) of the STM Images of the Template Molecules and Grafted Species at the 1-Phenyloctane/Graphite Interface.

template molecule	reduction potential (V) [a] in CV	I_D/I_G determined by Raman spectroscopy	pore-to-pore distance of the template network	periodicity grafted molecular species[b]
none (bare HOPG)	−0.16	0.067 ± 0.002	none	none
none (with 1-phenyloctane)	−0.15	0.074 ± 0.001	none	none
DBA-OC4	−0.16	0.050 ± 0.003	2.4 ± 0.1 nm	2.3 ± 0.1 nm
DBA-OC6	−0.15	0.059 ± 0.005	2.8 ± 0.1 nm	2.7 ± 0.1 nm
DBA-OC8	−0.16	0.058 ± 0.002	3.1 ± 0.1 nm	3.0 ± 0.1 nm

[a] Peak current potentials (E_{pc}s, vs. Ag/AgCl). [b] To detect the grafted molecular species, only the bright spots with an apparent height higher than 150 pm in the STM images are analyzed. Darker parts including the DBA cores (less than 100 pm in height) are excluded in this FFT analysis (Figure S12).

Next, nanopatterned covalent grafting was attempted under phase separated solution double layer conditions using a solution of **DBA-OCn** in 1-phenyloctane (30 μL) as an interfacial solvent layer. The **DBA-OCn** template layers were formed under the conditions described above, followed by the EC treatment to generate the aryl radicals.

In the case of **DBA-OC8** as template molecule, a large irreversible wave at –0.16 V was recorded in CV (Figure 5a). The reduction peak potential is comparable to that without the template molecules. Raman spectroscopic characterization confirms the appearance of the D-peak at 1350 cm^{-}

[1] and I_D/I_G value is 0.058 ± 0.002, indicating covalent bond formation (Figure 5b). The I_D/I_G value is slightly smaller compared to the conditions without the template molecule (0.074). Evidence for the templating effects comes from the STM images. Individual trimethoxyphenyl units are observed as bright features arranged in a hexagonal manner (Figure 5c). A 2D-FFT of the STM image clearly shows the hexagonal periodicity of trimethoxyphenyl molecular units with a mean periodicity of 3.0 ± 0.1 nm (Figure 5c: inset). This value matches the pore-to-pore distance of the **DBA-OC8** molecular network (3.1 ± 0.1 nm, Table 1). Sometimes, both the covalently attached trimethoxyphenyl units and adsorbed DBA molecules could be visualized at the same time (Figure 5d). Template-guided grafting was also observed using a solution of **DBA-OC6** (2.0×10^{-5} M) in 1-phenyloctane as a buffer layer (Figures S5 and S6). In this case, the hexagonal periodicity determined by 2D-FFT becomes 2.7 ± 0.1 nm, which also agrees with the pore-to-pore distance of **DBA-OC6** molecular network (2.8 ± 0.1 nm). Using a solution of **DBA-OC4** in 1-phenyloctane (5.0×10^{-5} M) as a buffer layer, only weak hexagonal periodicity of 2.3 ± 0.1 nm was observed in the STM images and 2D-FFT analysis (Figures S7 and S8). The guiding effect by the **DBA-OC4** network is therefore limited, which is attributed to the too small pore size formed by **DBA-OC4** (vide supra).

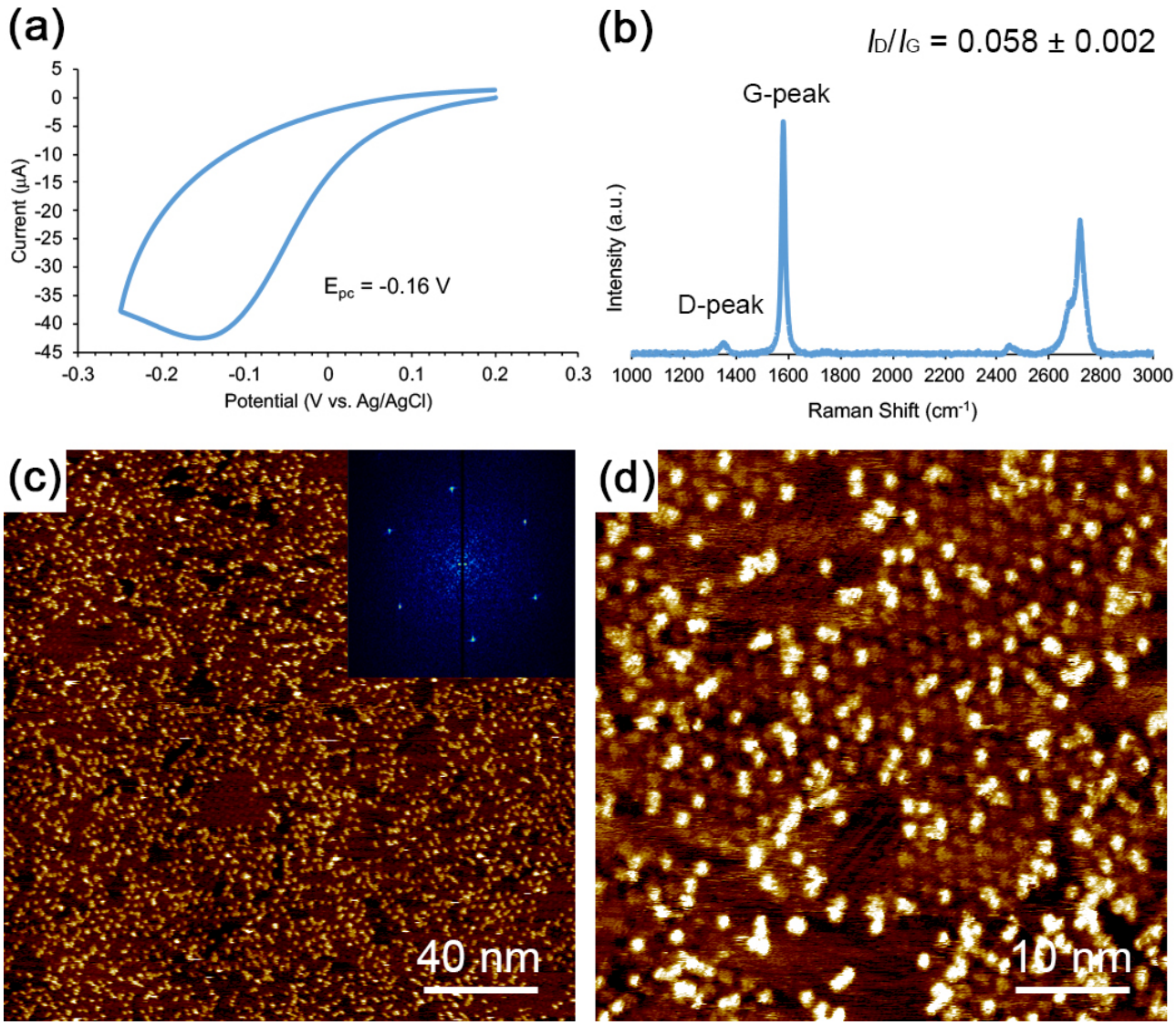

Figure 5. (a) Cyclic voltammogram during EC grafting of graphite using TMeOD in the presence of a solution of **DBA-OC8** in 1-phenyloctane as an interfacial layer. (b) Raman spectrum of the functionalized surface after drying. Excitation laser wavelength is 532 nm. Mean I_D/I_G is 0.058 ± 0.002. (c, d) STM images of functionalized graphite surface after **DBA-OC8** templated grafting in 1-phenyloctane. (c) Large area image (V_{bias} = −0.80 V, I_{set} = 30 pA). The inset corresponds to the 2D-FFT image. Six bright spots in the 2D-FFT image confirm the hexagonal periodicity. (d) Small area image (V_{bias} = −0.80 V, I_{set} = 30 pA).

Removing the physisorbed SAMN template is possible, using hot toluene (20 mL, 100 ºC). In case of **DBA-OC6** as template molecule, the I_D/I_G value becomes 0.049 ± 0.003, which is slightly smaller than the value before washing (I_D/I_G = 0.059 ± 0.005). Subsequent STM imaging of the sample shows that the covalently bound aryl units remain on the surface, while none of the DBA molecules were observed (Figure S11).

Pattern Transfer Fidelity and Mechanism

In order to qualitatively and semi-quantitatively evaluate the fidelity of the templated grafting, in other words to what extent does the periodicity of the pattern formed by the grafted molecules match the structural parameters of the SAMN template, STM images of the functionalized surfaces are analyzed by two approaches. One approach analyzes the position of each grafted molecular unit with respect to the template DBA. The other approach checks the global correspondence of the position of each grafted molecular unit to an ideal hexagonal alignment. On the basis of these analyses, here, we discuss the pattern transfer fidelity.

In the first approach, we analyzed the location of the bright features with respect to the DBA honeycomb networks using small area STM images of the functionalized surfaces where both the grafted aryl units and DBA molecules were visualized, as illustrated for **DBA-OC8** as the template (Figure 6a). The equivalent analyses for the other template molecules, **DBA-OC4** and **DBA-OC6**, are shown in Supporting Information (Figures S13 and S14). In Figure 6b, white tapes of 1 nm width overlaid on the image connect the triangular cores of **DBA-OC8** representing the porous network. Obviously, the DBA network does not extend over the full surface, as the networks are often disturbed by the grafted species.[54] In addition to the hexagons, there are also a very few pentagons and heptagons. In the case of the **DBA-OC8** template network, the hexagonal pores contain different numbers of bright features: 65% are vacant, 20% contain one bright feature, 12% two bright features, 1% three bright features, and <1% four bright features (Figure 6c and Table 2). The distributions for the other template molecules **DBA-OC4** and **DBA-OC6** are summarized in Table 2. The number of

the pores containing grafted aryl groups increases upon the pore size enlargement, while only for **DBA-OC8** in some pores more than two bright features appear. Though this analysis only affords limited local information, such pore size dependency indicates that the pore size is too small for **DBA-OC4**, yet slightly too large for **DBA-OC8**, which agrees with the molecular model estimation (vide supra).

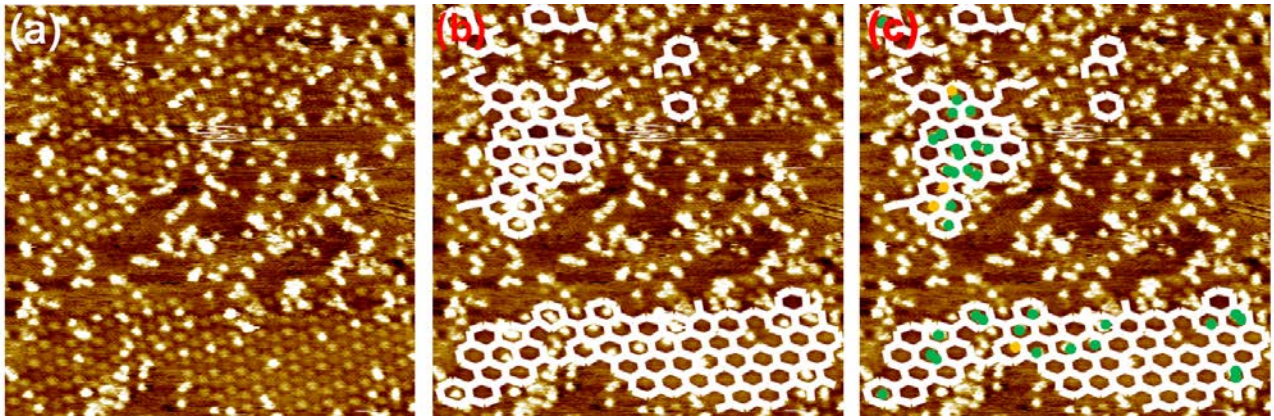

Figure 6. High resolution STM image (50 nm × 50 nm) of the functionalized graphite surface using **DBA-OC8** as template molecules. (a) original image, (b) image with white tapes that connect DBA cores, and (c) image with green and yellow disks. Green disks indicate bright features within the pores. Yellow dots indicate bright features that overlap with white tapes.

Table 2. Summary of the Distributions of the Pores Containing the Bright Features.

template molecule	number of bright features in hexagonal pores				
	0	1	2	3	4
DBA-OC4[a]	90%	8%	2%	0%	0%
DBA-OC6[b]	86%	11%	3%	0%	0%
DBA-OC8	65%	20%	12%	1%	<1%

[a] In addition to the hexagonal pores, there are pentagonal and heptagonal pores (1% and 2%, respectively). [b] A very few pentagonal pores exist too (<1%).

As the second approach, the global correspondence of the position of each grafted molecular unit to an ideal hexagonal alignment is analyzed. Details of the analysis procedure are described in the Supporting Information (Figures S15–S18, Table S2). This analysis also supports the hexagonal periodicities of the grafted aryl units.

Based on this analysis, the appearance of the hexagonal periodicities by the grafted molecular units can be attributed to preferential covalent bond formation in the pores. At the liquid/graphite interface, solvent molecules are co-adsorbed or at least transiently occupy the pores through adsorption-desorption dynamics,[55,56] yet such solvent molecules have not been directly visualized in the STM images. Because of such dynamic pore environment, the aryl radical or aryldiazonium ion can access the substrate (electrode) surface with small potential barrier for the electron transfer compared to other areas covered with the immobilized template molecules. As such, grafting preferentially occurs in the pores of the template network leading to the pattern transfer.

Chirality Transfer

As mentioned above, achiral **DBA-OCn**s form domains of opposite handedness, chiral *CW* and *CCW* honeycomb structures (Figures 1c and 2), and this supramolecular chirality goes along by an offset between the unit cell vector and the normal to a main symmetry axis of graphite (angle α).[48,54] In the case of **DBA-OC6**, the absolute value of the angle α determined for each domain using several independent images is ±6.3 ± 0.7°. The angle between the unit cell vectors of the *CW* and *CCW* structures, which we define as β, is calculated to be ca. 13° directly from 2D FFT analysis of an STM image including *CW* and *CCW* domains (Figure S19). This chirality information transfer to the location of the covalently attached aryl groups is an intriguing topic for the production of one-

sided or supratopically functionalized carbon surfaces with controlled chirality. Namely, as shown in Figure 1c, the angle between the SAMN unit cell vectors (blue rhombi) and the directions normal to the main symmetry axes of graphite (indicated in light green) is non-zero. Although the grafted patterns (red dots) by themselves are achiral (plane group *p*6*m*), given the grafting occurs at the center of the pores, the off-set of the SAMN unit cell renders the functionalized surface locally chiral when using achiral **DBA-OCn**s forming domains of both handedness. Moreover, the grafted patterns will become globally homochiral upon the use of supramolecular template layers of unique handedness (left or right half of Figure 1d).

In large area STM images of the functionalized graphite surface using **DBA-OC6** as a template molecule, we occasionally observed two different orientations in the hexagonal alignment of the grafted aryl group. The boundary between two such domains is highlighted by a blue line (Figure 7a). A corresponding 2D-FFT image shows two sets of hexagonal periodicities, and the angle between these two hexagonal periodicities is 14 ± 2° (Figures 7b,c). Note that this value agrees with the angle β of the template **DBA-OC6** network within experimental error. To directly prove the orientation of the grafted nanopatterns with respect to the substrate lattice underneath, we compared the 2D-FFTs of the grafted nanopatterns and of the graphite lattice, in the same STM image (see Figure S23). This analysis for 33 STM images unambiguously showed the same off-set of the unit cell vector of the grafted nanopattern and the normal to a main symmetry axis of graphite, *i.e.* +6.5 ± 0.5° or −6.6 ± 0.4°, as found for the **DBA-OC6** SAMN (±6.3 ± 0.7°). As expected, the "positive" and "negative" domains appear with almost equal frequency (section 12 in Supporting Information). This analysis concludes that the handedness (orientation) of the template network is successfully transferred to the surface location of the covalently attached aryl units (Figure 1c).

The above results suggest the possibility of orientational selection of the nanopattern with respect to the substrate lattice, to create a globally homochiral grafted pattern. To create supramolecular template layers of unique handedness, a requisite for the formation of homochiral grafted patterns later on, we designed and synthesized DBA **cDBA-OC6(*S*)-OC6**, a chiral template

molecule, having three chiral OC6(*S*) chains with methyl groups attached to stereogenic centers and three achiral OC6 chains.[41,57] Indeed, **cDBA-OC6(*S*)-OC6** exclusively forms a *CCW* honeycomb structure at 1,2,4-trichlorobenzene (TCB)/graphite interface after annealing treatment at 80 °C for 5 h (2.0×10^{-5} M, Figure S20). The three chiral chains are located at the rims of the hexagonal pores because of steric demands (Figure 8a,b).[57] Unit cell parameters are a = b = 3.2 ± 0.1 nm and γ = 60 ± 1°, which are identical to those of **DBA-OC6**. However, the angle α measures only negative values of −6.7 ± 0.8°, consistent with the homochirality of the network. Nanopatterned covalent grafting was attempted under phase separated solution double layer conditions using a solution of **cDBA-OC6(*S*)-OC6** in TCB (40 μL) as an interfacial solvent layer (Figure S22). STM observations of the functionalized graphite surface at the TCB/graphite interface revealed that individual trimethoxyphenyl units arranged in a hexagonal manner (Figures 8c and S22c), which is confirmed by the corresponding 2D-FFT with a hexagonal periodicity of 2.6 ± 0.1 nm (Figures 8c and S22c, insets). Furthermore, in agreement with the unique handedness of the **cDBA-OC6(*S*)-OC6** SAMN leading to a homochiral supramolecular network, the grafted pattern matches exactly the orientation (−6.8 ± 0.4 based on 24 STM images) of the template SAMN, rendering the covalently functionalized graphite surface homochiral (Figure 1d, Figure S25).

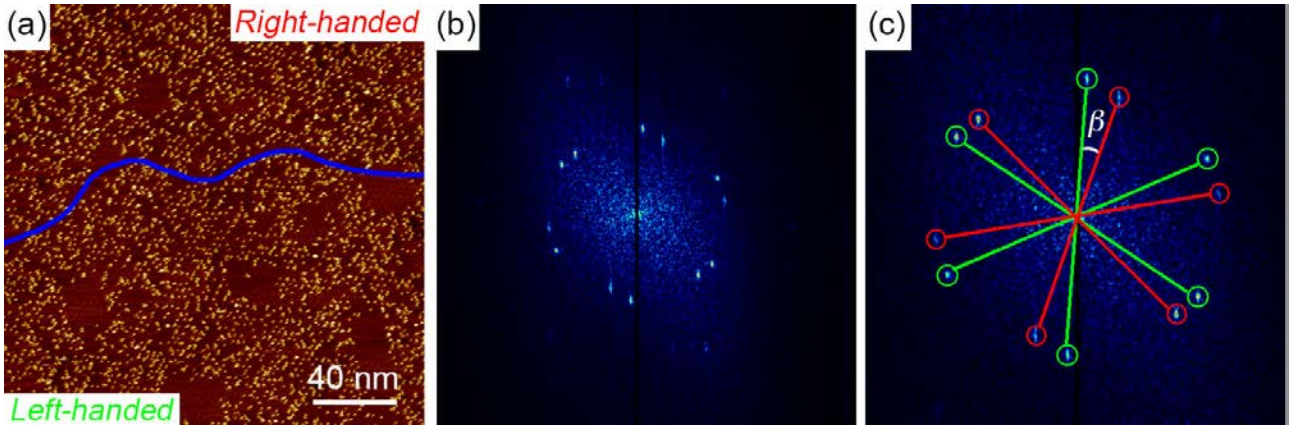

Figure 7. (a) Large area STM image of the functionalized graphite surface around the domain boundary after **DBA-OC6** templated grafting in 1-phenyloctane (V_{bias} = −0.60 V, I_{set} = 30 pA). Blue line in (a) is a boundary of hexagonally aligned bright features with different orientations. (b, c) 2D-

FFT images of image (a). Two sets of six bright spots confirm two different orientations of the hexagonal alignments. These are distinguished in zoomed image (c) by green and red circles, each derived from the bottom and top domains of (a). The mean angle (β) between the green and red lines connecting the spots and the center of the image is 14 ± 2°.

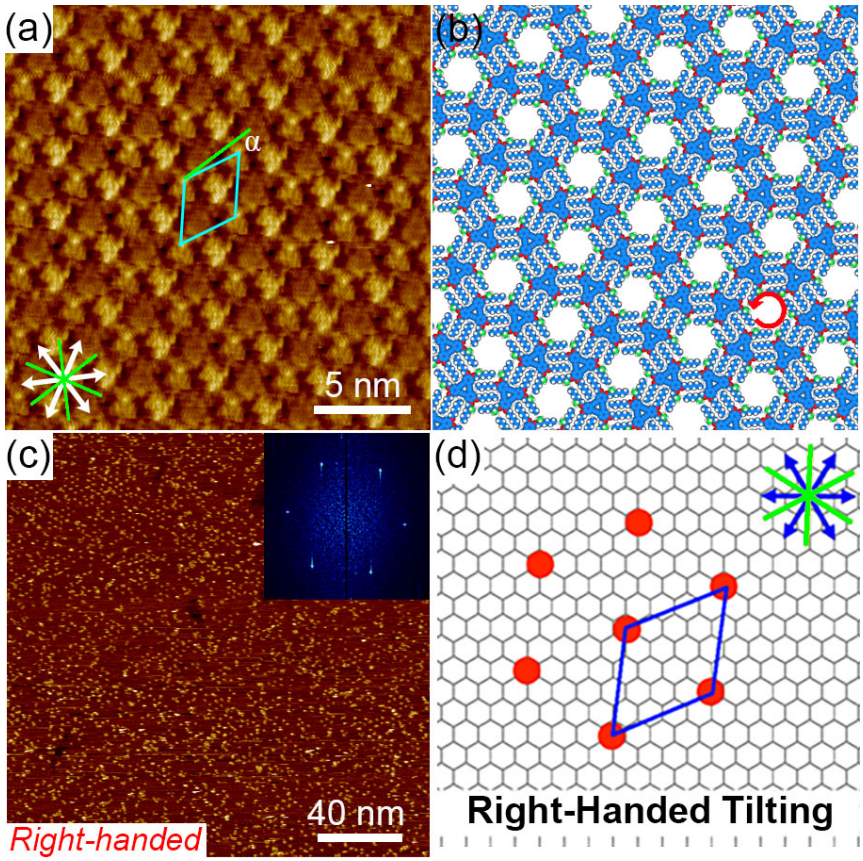

Figure 8. (a) STM image of a *CCW* honeycomb structure formed by **cDBA-OC6(*S*)-OC6** (V_{bias} = −0.44 V, I_{set} = 114 pA). White arrows and light green lines are main symmetry axes and their normals of a graphite substrate underneath. Turquoise rhombus is a unit cell. Angle α is between one of the unit cell vectors and the closest normal of the graphite lattice. (b) Molecular mechanics optimized (COMPASS force field) molecular models of the honeycomb structure of **cDBA-OC6(*S*)-OC6** on bilayered graphene sheets under periodic boundary conditions (PBCs; a = b = 3.25 nm and γ = 60.0°). The bilayered graphene sheets are omitted for clarity. The methyl groups attached to the stereogenic center are colored in light green. (c) Large area STM image of the functionalized graphite surface after **cDBA-OC6(*S*)-OC6** templated grafting in TCB (V_{bias} = −0.60 V, I_{set} = 30 pA). The inset

corresponds to the 2D-FFT image. A set of six bright spots in the 2D-FFT image confirms the hexagonal periodicity. (d) Schematic drawing of the chiral-position controlled functionalized surface. The red dots correspond to grafted aryl units. Blue arrows and light green lines are main symmetry axes and their normals of a graphite substrate. For clarity, the unit cell vectors of the grafted pattern, and the graphite lattice are not to scale.

CONCLUSIONS

We herein report, for the first time, that porous self-assembled molecular networks act as nanometer scale template for the covalent EC functionalization of graphite using an aryldiazonium salt. Hexagonally aligned grafted species on graphite surfaces with lateral periodicity of 2.3, 2.7, and 3.0 nm were achieved utilizing molecular templates of different pore sizes. The template network can be removed by washing with a common organic solvent. The local and global analyses support that the pattern transfer fidelity is influenced by the pore size. This implies fidelity improvement will be possible by selecting porous SAMN templates with suitable pore shape and size. We suggest that the pattern transfer is attributed to the dynamic pore environment at the liquid/graphite interface. Finally, we confirmed that the well-defined orientation of the porous template network is transferred to the alignment of the supratopically grafted species along non-symmetry axes of graphite. This demonstrates the first covalent functionalization of a carbon surface in a chiral manner. The understanding of the chemical functionalization of graphite or graphene and its impact on the electronic and surface properties, are important for the production of tailored carbon materials.[58–60] Additionally, the production of homochiral graphite surfaces or graphene materials would open various possibilities in carbon materials science.[43,61,62]

ASSOCIATED CONTENT

Supporting Information

The Supporting Information is available free of charge on the ACS Publications website.

Experimental Details, MM Simulations, Additional STM images, Additional Raman Spectra, Details of Positional Analysis.

AUTHOR INFORMATION

Corresponding Author

*tahara@meiji.ac.jp

*steven.defeyter@kuleuven.be

*tobe@chem.es.osaka-u.ac.jp

ORCID

Kazukuni Tahara: 0000-0002-3634-541X

Hiromasa Kaneko: 0000-0001-8367-6476

Steven De Feyter: 0000-0002-0909-9292

Yoshito Tobe: 0000-0002-1795-5829

Brandon Hirsch: 0000-0002-3452-0990

Note

The authors declare no competing financial interest.

Acknowledgement

This work is supported by JST-PRESTO “Molecular technology and creation of new functions”, JSPS KAKENHI (JP15H02164, JP17H04794), the Fund of Scientific Research Flanders (FWO), and KU Leuven - Internal Funds. B.E.H. thanks FWO for a postdoctoral fellowship and the Belgian-American Educational Foundation. A.B. thanks FWO for a personal fellowship (SBO).

References

(1) Barth, J. V.; Costantini, G.; Kern, K. Engineering Atomic and Molecular Nanostructures at Surfaces. *Nature* **2005**, *437*, 671–679.

(2) Palma, C.-A.; Samorì, P. Blueprinting Macromolecular Electronics. *Nat. Chem.* **2011**, *3*, 431–436.

(3) McCreery, R.; Bergren, A. J. Diazonium Compounds in Molecular Electronics. In *Aryl Diazonium Salts*; Chehimi, M. M. Ed.; Wiley-VCH Verlag & Co. KGaA: Weinheim, 2012; pp 219–239.

(4) Assresahegn, B. D.; Brousse, T.; Belanger, D. Advances on the Use of Diazonium Chemistry for Functionalization of Materials Used in Energy Storage Systems. *Carbon* **2015**, *92*, 362–381.

(5) Guo, L.; Zhang, Y.; Wang, J.; Ma, L.; Ma, S.; Zhang, Y.; Wang, E.; Bi, Y.; Wang, D.; McKee, W. C.; Xu, Y.; Chen, J.; Zhang, Q.; Nan, C.; Gu, L.; Bruce, P. G.; Peng, Z. Unlocking the Energy Capabilities of Micron-Sized $LiFePO_4$. *Nat. Commun.* **2015**, 6, 7898.

(6) Cao, C.; Zhang, Y.; Jiang, C.; Qi, M.; Liu, G. Advances on Aryldiazonium Salt Chemistry Based Interfacial Fabrication for Sensing Applications. *ACS Appl. Mater. Interfaces* **2017**, *9*, 5031–5049.

(7) Downard, A. J.; Gross, A. J.; Simons, B. M. Patterned Molecular Layers on Surfaces. In *Aryl Diazonium Salts*; Chehimi, M. M. Ed.; Wiley-VCH Verlag & Co. KGaA: Weinheim, 2012; pp 53–69.

(8) Belmont, J. A.; Bureau, C.; Chehimi, M. M.; Gam-Derouich, S.; Pinson, J. Patents and Industrial Applications of Aryl Diazonium Salts and Other Coupling Agents. In *Aryl Diazonium Salts*; Chehimi, M. M. Ed.; Wiley-VCH Verlag & Co. KGaA: Weinheim, 2012; pp 309–321.

(9) Bottari, G.; Herranz, M. Á.; Wibmer, L.; Volland, M.; Rodríguez-Pérez, L.; Guldi, D. M.; Hirsch, A.; Martín, N.; D'Souza, F.; Torres, T. Chemical Functionalization and Characterization of Graphene-Based Materials. *Chem. Soc. Rev.* **2017**, *46*, 4464–4500.

(10) Bai, J.; Zhong, X.; Jiang, S.; Huang, Y.; Duan, X. Graphene Nanomesh. *Nat. Nanotechnol.* **2010**, *5*, 190–194.

(11) Sun, Z.; Pint, C. L.; Marcano, D. C.; Zhang, C.; Yao, J.; Ruan, G.; Yan, Z.; Zhu, Y.; Hauge, R. H.; Tour, J. M. Towards Hybrid Superlattices in Graphene. *Nat. Commun.* **2011**, *2*, 559.

(12) Tracz, A.; Wegner, G.; Rabe, J. P. Scanning Tunneling Microscopy Study of Graphite Oxidation in Ozone-Air Mixtures. *Langmuir* **2003**, *19*, 6807–6812.

(13) Eigler, S.; Hirsch, A. Chemistry with Graphene and Graphene Oxide–Challenges for Synthetic Chemists. *Angew. Chem. Int. Ed.* **2014**, *53*, 7720–7738.

(14) Wu, J.; Xie, L.; Li, Y.; Wang, H.; Ouyang, Y.; Guo, J.; Dai, H. Controlled Chlorine Plasma Reaction for Noninvasive Graphene Doping. *J. Am. Chem. Soc.* **2011**, *133*, 19668–19671.

(15) Kariuki, J. K.; McDermott, M. T. Nucleation and Growth of Functionalized Aryl Films on Graphite Electrodes. *Langmuir* **1999**, *15*, 6534–6540.

(16) Park, J.; Yan, M. Covalent Functionalization of Graphene with Reactive Intermediates. *Acc. Chem. Res.* **2013**, *46*, 181–189.

(17) Navarro, J. J.; Calleja, F.; Miranda, R.; Pérez, E. M.; Vázquez de Parga, A. L. High Yielding and Extremely Site-Selective Covalent Functionalization of Graphene. *Chem. Commun.* **2017**, *53*, 10418−10421.

(18) Navarro, J. J.; Leret, S.; Calleja, F.; Stradi, D.; Black, A.; Bernardo-Gavito, R.; Garnica, M.; Granados, D.; Vázquez de Parga, A. L.; Pérez, E. M.; Miranda, R. Organic Covalent Patterning of Nanostructured Graphene with Selectivity at the Atomic Level. *Nano Lett.* **2016**, *16*, 355–361.

(19) Galli, C. Radical Reactions of Arenediazonium Ions: An Easy Entry into the Chemistry of the Aryl Radical. *Chem. Rev.* **1988**, *88*, 765–792.

(20) Berisha, A.; Chehimi, M. M.; Pinson, J.; Podvorica, F. I. Electrode Surface Modification using Diazonium Salts. In *Electroanalytical Chemistry*; Bard, A. J., Zoski, C. G., Eds.; CRC Press; Taylor & Francis Group: New York, 2016; Vol. 26, pp 115–223.

(21) Mohamed, A. A.; Salmi, Z.; Dahoumane, S. A.; Mekki, A.; Carbonnier, B.; Chehimi, M. M. Functionalization of Nanomaterials with Aryldiazonium Salts. *Adv. Colloid Interface Sci.* **2015**, *225*, 16–36.

(22) Allongue, P.; Delamar, M.; Desbat, B.; Fagebaume, O.; Hitmi, R.; Pinson, J.; Savéant, J. M. Covalent Modification of Carbon Surfaces by Aryl Raicals Generated from Electrochemical Reduction of Diazonium Salts. *J. Am. Chem. Soc.* **1997**, *119*, 201–207.

(23) Combellas, C.; Jiang, D.; Kanoufi, F.; Pinson, J.; Podvorica, F. I. Steric Effects in the Reaction of Aryl Radicals on Surfaces. *Langmuir* **2009**, *25*, 286–293.

(24) Mattiuzzi, A.; Jabin, I.; Mangeney, C.; Roux, C.; Reinaud, O.; Santos, L.; Bergamini, J.-F.; Hapiot, P.; Lagrost, C. Electrografting of Calix[4]arenediazonium Salts to Form Versatile Robust Platforms for Spatially Controlled Surface Functionalization. *Nat. Commun.* **2012**, *3*, 1130.

(25) Greenwood, J.; Phan, T. H.; Fujita, Y.; Li, Z.; Ivasenko, O.; Vanderlinden, W.; Van Gorp, H.; Frederickx, W.; Lu, G.; Tahara, K.; Tobe, Y.; Uji-i, H.; Mertens, S. F. L.; De Feyter, S. Covalent

Modification of Graphene and Graphite Using Diazonium Chemistry: Tunable Grafting and Nanomanipulation. *ACS Nano* **2015**, *9*, 5520–5535.

(26) Tahara, K.; Kubo, Y.; Lindner, B.; Hashimoto, S.; Hirose, S.; Brown, A.; Hirsch, B.; Daukiya, L.; De Fetyer, S.; Tobe, Y. Steric and Electronic Effects of Electrochemically Generated Aryl Radicals on Grafting of the Graphite Surface. *Langmuir* **2019**, *35*, 2089–2098.

(27) Corgier, B. P.; Bélanger, D. Electrochemical Surface Nanopatterning Using Microspheres and Aryldiazonium. *Langmuir* **2010**, *26*, 5991–5997.

(28) Zhou, L.; Liao, L.; Wang, J.; Yu, J.; Li, D.; Xie, D.; Xie, Q.; Liu, Z.; Yang, Y.; Guo, X.; Liu, Z. Substrate-Induced Graphene Chemistry for 2D Superlattices with Tunable Periodicities. *Adv. Mater.* **2016**, *28*, 2148–2154.

(29) Gross, A. J.; Nock, V.; Polson, M. I. J.; Alkaisi, M. M.; Downard, A. J. Surface Patterning Using Two-Phase Laminar Flow and in situ Formation of Aryldiazonium Salts. *Angew. Chem. Int. Ed.* **2013**, *52*, 10261–10264.

(30) Wang, Q. H.; Jin, Z.; Kim, K. K.; Hilmer, A. J.; Paulus, G. L. C.; Shih, C.-J.; Ham, M.-H.; Sanchez-Yamagishi, J. D.; Watanabe, K.; Taniguchi, T.; Kong, J.; Jarillo-Herrero, P.; Strano, M. S. Understanding and Controlling the Substrate Effect on Graphene Electron-Transfer Chemistry via Reactivity Imprint Lithography. *Nat. Chem.* **2012**, *4*, 724–732.

(31) Lehr, J.; Garrett, D. J.; Paulik, M. G.; Flavel, B. S.; Brooksby, P. A.; Williamson, B. E.; Downard, A. J. Patterning of Metal, Carbon, and Semiconductor Substrates with Thin Organic Films by Microcontact Printing with Aryldiazonium Salt Inks. *Anal. Chem.* **2010**, *82*, 7027–7034.

(32) Phan, T. H.; Van Gorp, H.; Li, Z.; Huynh, T. M. T.; Fujita, Y.; Verstraete, L.; Eyley, S.; Thielemans, W.; Uji-i, H.; Hirsch, B. E.; Mertens, S. F. L.; Greenwood, J.; Ivasenko, O.; De Feyter, S. Graphite and Graphene Fairy Circles: A Bottom-Up Approach for the Formation of Nanocorrals *ACS Nano* **2019**, *13*, 5559–5571.

(33) Xia, Z.; Leonardi, F.; Gobbi, M.; Liu, Y.; Bellani, V.; Liscio, A.; Kovtun, A.; Li, R.; Feng, X.; Orgiu, E.; Samorì, P.; Treossi, E.; Palermo, V. Electrochemical Functionalization of Graphene at the Nanoscale with Self-Assembling Diazonium Salts. *ACS Nano* **2016**, *10*, 7125–7134.

(34) Tahara, K.; Ishikawa, T.; Hirsch, B. E.; Kubo, Y.; Brown, A.; Eyley, S.; Daukiya, L.; Thielemans, W.; Li, Z.; Walke, P.; Hirose, S.; Hashimoto, S.; De Feyter, S.; Tobe, Y. Self-Assembled Monolayers as Templates for Linearly Nanopatterned Covalent Chemical Functionalizaiton of Graphite and Graphene Surfaces. *ACS Nano* **2018**, *12*, 11520–11528.

(35) Elemans, J. A. A. W.; Lei, S.; De Feyter, S. Molecular and Supramolecular Networks on Surfaces: From Two-Dimensional Crystal Engineering to Reactivity. *Angew. Chem. Int. Ed.* **2009**, *48*, 7298–7332.

(36) Goronzy, D. P.; Ebrahimi, M.; Rosei, F.; Arramel; Fang, Y.; De Feyter, S.; Tait, S. L.; Wang, C.; Beton, P. H.; Wee, A. T. S.; Weiss, P. S.; Perepichka, D. F. Supramolecular Assemblies on Surfaces: Nanopatterning, Functionality, and Reactivity. *ACS Nano* **2018**, *12*, 7445–7481.

(37) Bonifazi, D.; Mohnani, S.; Llanes-Pallas, A. Supramolecular Chemistry at Interfaces: Molecular Recognition on Nanopatterned Porous Surfaces. *Chem. Eur. J.* **2009**, *15*, 7004–7025.

(38) Zang, X.M., Z.; Zeng Q.D.; Wang, C. Host-Guest Supramolecular Chemistry at Solid-Liquid Interface: An Important Strategy for Preparing Two-Dimensional Functional Nanostructures. *Science China-Chemistry* **2014**, *57*, 13–25.

(39) Kudernac, T.; Lei, S.; Elemans, J. A. A. W.; De Feyter, S. Two-Dimensional Supramolecular Self-Assembly: Nanoporous Networks on Surfaces. *Chem. Soc. Rev.* **2009**, *38*, 402–421.

(40) Madueno, R.; Räisänen, M. T.; Silien, C.; Buck, M. Functionalizing Hydrogen-Bonded Surface Networks with Self-Assembled Monolayers. *Nature* **2008**, *454*, 618–621.

(41) Tahara, K.; Yamaga, H.; Ghijsens, E.; Inukai, K.; Adisoejoso, J.; Blunt, M. O.; De Feyter, S.; Tobe, Y. Control and Induction of Surface-Confined Homochiral Porous Molecular Networks. *Nat. Chem.* **2011**, *3*, 714–719.

(42) Chen, T.; Yang, W.-H.; Wang, D.; Wan, L.-J. Globally Homochiral Assembly of Two-Dimensional Molecular Networks Triggered by Co-Adsorbers. *Nat. Commun.* **2013**. *4*, 1389.

(43) Liu, X.; Zhang, Z.; Guo, W. Universal Rule on Chirality-Dependent Bandgaps in Graphene Antidot Lattices. *Small* **2013**, *9*, 1405–1410.

(44) Lorenzo, M. O.; Baddeley, C. J.; Muryn, C.; Raval, R. Extended Surface Chirality from Supramolecular Assemblies of Adsorbed Chiral Molecules. *Nature* **2000**, *404*, 376–379.

(45) Tahara, K.; Furukawa, S.; Uji-i, H.; Uchino, T.; Ichikawa, T.; Zhang, J.; Mamdouh, W.; Sonoda, M.; De Schryver, F. C.; De Feyter, S.; Tobe, Y. Two-Dimensional Porous Molecular Networks of Dehydrobenzo[12]annulene Derivatives via Alkyl Chain Interdigitation. *J. Am. Chem. Soc.* **2006**, *128*, 16613–16625.

(46) Lei, S.; Tahara, K.; De Schryver, F. C.; Van der Auweraer, M.; Tobe, Y.; De Feyer, S. One Building Block, Two Different Supramolecular Surface-Confined Patterns: Concentration in Control at the Solid-Liquid Interface. *Angew. Chem. Int. Ed.* **2008**, *47*, 2964–2968.

(47) Blunt, M. O.; Adisoejoso, J.; Tahara, K.; Katayama, K.; Van der Auweraer, M.; Tobe, Y.; De Feyter, S. Temperature-Induced Structural Phase Transitions in a Two-Dimensional Self-Assembled Network. *J. Am. Chem. Soc.* **2013**, *135*, 12068–12075.

(48) Ghijsens, E.; Ivasenko, O.; Tahara, K.; Yamaga, H.; Itano, S.; Balandina, T.; Tobe, Y.; De Feyter, S. A Tale of Tails: Alkyl Chain Directed Formation of 2D Porous Networks Reveals Odd-Even Effects and Unexpected Bicomponent Phase Behavior. *ACS Nano* **2013**, *7*, 8031–8042.

(49) Hirsch, A.; Hauke, F. Post-Graphene 2D Chemistry: The Emerging Field of Molybdenum Disulfide and Black Phosphours Functionalization. *Angew. Chem. Int. Ed.* **2018**, *57*, 4338–4354.

(50) Plass, K. E.; Grzesiak, A. L.; Matzger, A. J. Molecular Packing and Symmetry of Two-Dimensional Crystals. *Acc. Chem. Res.* **2007**, *40*, 287–293.

(51) Lazzaroni, R.; Calderone, A.; Lambin, G.; Rabe, J. P.; Brédas, J. L. A Theoretical Approach to the STM Imaging of Adsorbates on the Graphite Surface. *Synth. Met.* **1991**, *41*, 525–528.

(52) Elemans, J. A. A. W.; De Cat. I.; Xu, H.; De Feyter, S. Two-Dimensional Chirality at Liquid-Solid Interfaces. *Chem. Soc. Rev.* **2009**, *38*, 722–736.

(53) Tuinstra, F.; Koenig, J. L. Raman Spectrum of Graphite. *J. Chem. Phys.* **1970**, *53*, 1126–1130.

(54) Bragança, A. M.; Hirsch, B. E.; Sanz-Matias, A.; Hu, Y.; Walke, P.; Tahara, K.; Harvey, J. N.; Tobe, Y.; De Feyter, S. How Does Chemisorption Impact Physisorption? Molecular View of Defect Incorporation and Perturbation of Two-Dimensional Self-Assembly. *J. Phys. Chem. C* **2018**, *122*, 24046–24054.

(55) Tahara, K.; Kaneko, K.; Katayama, K.; Itano, S.; Nguyen, C. H.; Amorim, D. D. D.; De Feyter, S.; Tobe, Y. Formation of Multicomponent Star Structures at the Liquid/Solid Interface. *Langmuir* **2015**, *31*, 7032–7040.

(56) Eder, G.; Kloft, S.; Martsinovich, N.; Mahata, K.; Schmittel, M.; Heckl, W. M.; Lackinger, M. Incorporation Dynamics of Molecular Guests into Two-Dimensional Supramolecular Host Networks at the Liquid-Solid Interface. *Langmuir* **2011**, *27*, 13563–13571.

(57) Tahara, K.; Noguchi, A.; Nakayama, R.; Ghijsens, E.; De Feyter, S.; Tobe, Y. Reversing the Handedness of Self-Assembled Porous Molecular Networks through the Number of Identical Chiral Centres. *Angew. Chem. Int. Ed.* **2019**, *58*, 7733–7738.

(58) Ferrari, A. C.; Bonaccorso, F.; Fal'ko, V.; Novoselov, K. S.; Roche, S.; Bøggild, P.; Borini, S.; Koppens, F. H. L.; Palermo, V.; Pungo, N.; Garrido, J. A.; Sordan, R.; Bianco, A.; Ballerini, L.; Prato, M.; Lidorikis, E.; Kivioja, J.; Marinelli, C.; Ryhänen, T.; Morpurgo, A.; Coleman, J. N.; Nicolosi, V.; Colombo, L.; Fert, A.; Garcia-Hernandez, M.; Bachtold, A.; Schneider, G. F.; Guinea, F.; Dekker, C.; Barbone, M.; Sun, Z.; Galiotis, C.; Grigorenko, A. N.; Konstantatos, G.; Kis, A.; Katsnelson, M.; Vandersypen, L.; Loiseau, A.; Morandi, V.; Neumaier, D.; Treossi, E.; Pellegrini, V.; Poloni, M.; Tredicucci, A.; Williams, G. M.; Hongm B. H.; Ahn, J.-H.; Kim, J. M.; Zirath, H.; van Wees, B. J.; van der Zant, H.; Occhipiniti, L.; Di Matteo, A.; Kinloch, I. A.; Seyller, T.; Quesnel, E.; Feng, X.; Teo, K.; Rupesinghe, N.; Hakonen, P.; Nei, S. R. T.; Tannock, Q.; Löfwander, T.; Kinaret, J. Science

and Technology Roadmap for Graphene, Related Two-Dimensional Crystals, and Hybrid Systems. *Nanoscale* **2015**, *7*, 4598–4810.

(59) García-Lastra, J. M. Strong Dependence of Band-Gap Opening at the Dirac Point of Graphene upon Hydrogen Adsorption Periodicity. *Phys. Rev. B* **2010**, *82*, 235418.

(60) Mirzadeh, M.; Farjam, M. First-Principles Study of Bandgap Effects in Graphene Due to Hydrogen Adsorption. *J. Phys.: Condens. Matter* **2012**, *24*, 235304.

(61) Purcell-Milton, F.; McKenna, R.; Brennan, L. J.; Cullen, C. P.; Guillemeney, L.; Tepliakov, N. V.; Baimuratov, A. S.; Rukhlenko, I. D.; Perova, T. S.; Duesberg, G. S.; Baranov, A. V.; Fedorov, A. V.; Gun'ko, Y. K. Induction of Chirality in Two-Dimensional Nanomaterials: Chiral 2D MoS_2 Nanostructures. *ACS Nano* **2018**, *12*, 954–964.

(62) Shen, B.; Kim, Y.; Lee, M. Supramolecular Chiral 2D Materials and Emerging Functions. *Adv. Mater.* **2020**, 1905669.

TOC Graphic

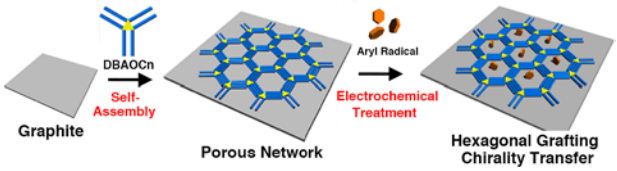
DBAOCn
Self-
Assembly
Graphite
Porous Network
Aryl Radical
Electrochemical
Treatment
Hexagonal Grafting
Chirality Transfer